Averaged transverse momentum correlations of hadrons in relativistic heavy-ion collisions

Yan-ting Feng,[1] Feng-lan Shao,[1,*] and Jun Song[2,†]

[1]*School of Physics and Physical Engineering, Qufu Normal University, Shandong 273165, China*

[2]*School of Physical Science and Intelligent Engineering, Jining University, Shandong 273155, China*

(Received 28 April 2022; revised 6 June 2022; accepted 9 September 2022; published 21 September 2022)

We compile experimental data for the averaged transverse momentum ($\langle p_T \rangle$) of proton, Λ, Ξ^-, Ω^-, and ϕ at midrapidity in Au+Au collisions at $\sqrt{s_{NN}} = 200$, 39, 27, 19.6, 11.5, 7.7 GeV and in Pb+Pb collisions at $\sqrt{s_{NN}} = 2.76$ TeV, and find that experimental data of these hadrons exhibit systematic correlations. We apply a quark combination model with equal-velocity combination approximation to derive analytic formulas of hadronic $\langle p_T \rangle$ in the case of exponential form of quark p_T spectra at hadronization. We use them to successfully explain the systematic correlations exhibited in $\langle p_T \rangle$ data of $p\Lambda$, $\Lambda\Xi^-$, $\Xi^-\Omega^-$, and $\Xi^-\phi$ pairs. We also use them to successfully explain the regularity observed in $\langle p_T \rangle$ of these hadrons as the function of $(dN_{\rm ch}/dy)/(0.5N_{\rm part})$ at midrapidity in central heavy-ion collisions at both Relativistic Heavy Ion Collider (RHIC) and Large Hadron Collider (LHC) energies. Our results suggest that the constituent quark degrees of freedom and the equal-velocity combination of these constituent quarks at hadronization play an important role in understanding $\langle p_T \rangle$ correlations of baryons and ϕ meson in heavy-ion collisions at these RHIC and LHC energies.

DOI: 10.1103/PhysRevC.106.034910

I. INTRODUCTION

In relativistic heavy-ion collisions, the hot nuclear matter is created at the early collision stage by the intensively inelastic collisions of colliding nucleons [1–6]. Subsequently, the matter expands, cools, and finally decomposes into hadrons scattering out. The evolution of hot nuclear matter is a complex process governed by nonperturbative QCD and is mainly modeled by hydrodynamic models [7] and transport models [8–10] at present. Hadrons produced from hot nuclear matter always have certain transverse momentum p_T, the component of momentum which is perpendicular to the beam direction. The p_T distributions of hadrons carry lots of information on hot nuclear matter such as thermalization and transverse collective flow generated by system expansion in both partonic and hadronic stages, and is an important physical observable in relativistic heavy-ion collision experiments.

Rich experimental data for the p_T spectra of identified hadrons at midrapidity have been successively reported in heavy-ion collisions at Relativistic Heavy Ion Collider (RHIC) and Large Hadron Collider (LHC) over the past decade [11–22]. Based on these experimental data, many studies on the properties of the hadronic p_T distribution have been carried out, which greatly improves people's understanding of the property of the created hot nuclear matter and the mechanism of hadron production in relativistic heavy-ion collisions [23–35]. The averaged transverse momentum ($\langle p_T \rangle$) of hadrons is obtained by integrating over p_T spectra of hadrons. It is dominated by the property of hadronic p_T spectra in the low p_T range, and therefore it reflects the property of soft hadrons, corresponding to that of hot nuclear matters.

In this paper, we study the property of $\langle p_T \rangle$ of identified hadrons produced in relativistic heavy-ion collisions. We compile the experimental data for the $\langle p_T \rangle$ of ϕ, protons, Λ, Ξ^-, and Ω^- at midrapidity in Au+Au collisions at $\sqrt{s_{NN}} =$ 200, 39, 27, 19.6, 11.5, 7.7 GeV and in Pb+Pb collisions at $\sqrt{s_{NN}} = 2.76$ TeV. We search the regularity in the $\langle p_T \rangle$ data of these hadrons and, in particular, their dependence on hadron species and collision energy. We discuss what underlying physics is responsible for the observed regularity. In particular, we study the effect of hadronization by an equal-velocity combination (EVC) mechanism of quarks and antiquarks [36–38] in explaining the experimental data of $\langle p_T \rangle$. We derive analytic expression for the $\langle p_T \rangle$ of identified hadrons in EVC mechanism so as to give a clear quark flavor dependence of the hadronic $\langle p_T \rangle$ and provide intuitive explanations of experimental data.

The paper is organized as follows. In Sec. II, we briefly introduce our EVC model and derive the $\langle p_T \rangle$ of identified hadrons for the simplified quark distributions at hadronization. In Sec. III, we show our findings for the systematic correlation among experimental data for $\langle p_T \rangle$ of hadrons in relativistic heavy-ion collisions and give an intuitive explanation using our EVC model. In Sec. IV, we show the regularity on the $\langle p_T \rangle$ of hadrons in central heavy-ion collisions as the function of $(dN_{\rm ch}/dy)/(0.5N_{\rm part})$. In Sec. V, we discuss the influence of resonance decays on the $\langle p_T \rangle$ correlations of hadrons. Finally, the summary and discussion are given in Sec. VI.

II. $\langle p_T \rangle$ OF HADRONS IN EVC MODEL

In this section, we apply a particular quark combination model [37–39] to describe the production of hadrons at hadronization and derive the $\langle p_T \rangle$ of hadrons. The model

*shaofl@mail.sdu.edu.cn

†songjun2011@jnxy.edu.cn

was proposed in Ref. [37] to explain the constituent QNS property that we found in the experimental data of p_T spectra of identified hadrons in pPb collisions at LHC energy. The model is now applied to pp, pA, and AA collisions at both RHIC and LHC energies, and has successfully explained the experimental data for yields, p_T spectra, and elliptic flow of light-flavor hadrons and those of single-charm hadrons at RHIC and LHC [38–45].

Here, we briefly introduce the main formulas of the model which are most relevant to derive $\langle p_T \rangle$ of hadrons. In the scenario of stochastic combination of quarks and antiquarks at hadronization, the momentum distribution of the formed hadron can be obtained by

$$f_{B_j}(p) = \int dp_1 dp_2 dp_3 \mathcal{R}_{B_j}(p_1, p_2, p_3; p)\, f_{q_1q_2q_3}(p_1, p_2, p_3), \tag{1}$$

$$f_{M_j}(p) = \int dp_1 dp_2 \mathcal{R}_{M_j}(p_1, p_2; p) f_{q_1\bar{q}_2}(p_1, p_2). \tag{2}$$

Here, $f_{q_1q_2q_3}(p_1, p_2, p_3)$ is the joint momentum distribution of $q_1q_2q_3$ and $f_{q_1\bar{q}_2}(p_1, p_2)$ is that of $q_1\bar{q}_2$. $\mathcal{R}_{B_j}(p_1, p_2, p_3; p)$ is the combination probability function of $q_1q_2q_3$ with momenta p_1, p_2, and p_3 forming a baryon B_j with momentum p_B. $\mathcal{R}_{M_j}(p_1, p_2; p)$ of the meson has similar meaning.

Because hadronization is a complex nonperturbative process, it is hard to know the complete information of quark properties at hadronization and their combination probability functions $\mathcal{R}_{B_j}(p_1, p_2, p_3; p)$ and $\mathcal{R}_{M_j}(p_1, p_2; p)$ from first-principles calculations. Here, the model assumes the constituent quarks and antiquarks as the effective degrees of freedom for the final parton system created in collisions at the hadronization stage. Based on the constituent quark model of the hadron structure at low-energy scale, the model takes the EVC of these constituent quarks and antiquarks as the main feature of hadron formation. The quark masses are taken as the constituent masses so the EVC of these constituent quarks and antiquarks can correctly construct the on-shell hadron. In EVC mechanisms, combination probability functions have relatively simple expressions

$$\mathcal{R}_{B_j}(p_1, p_2, p_3; p) = \kappa_{B_j} \prod_{i=1}^{3} \delta(p_i - x_i p), \tag{3}$$

$$\mathcal{R}_{M_j}(p_1, p_2; p) = \kappa_{M_j} \prod_{i=1}^{2} \delta(p_i - x_i p). \tag{4}$$

κ_{B_j} and κ_{M_j} are independent of momentum. Moment fraction $x_i = m_i/(m_1 + m_2 + m_3)$ $(i = 1, 2, 3)$ in baryon formula satisfies $x_1 + x_2 + x_3 = 1$ and $x_i = m_i/(m_1 + m_2)$ $(i = 1, 2)$ in meson formula satisfies $x_1 + x_2 = 1$. m_i is constituent mass of quark q_i and we take $m_u = m_d = 0.3$ GeV and $m_s = 0.5$ GeV.

We further assume the factorization approximation for joint momentum distributions $f_{q_1q_2q_3}(p_1, p_2, p_3) = f_{q_1}(p_1) f_{q_2}(p_2) f_{q_3}(p_3)$ and $f_{q_1\bar{q}_2}(p_1, p_2) = f_{q_1}(p_1) f_{\bar{q}_2}(p_2)$. Then, we have

$$f_{B_j}(p) = \kappa_{B_j} f_{q_1}(x_1 p) f_{q_2}(x_2 p) f_{q_3}(x_3 p), \tag{5}$$

$$f_{M_j}(p) = \kappa_{M_j} f_{q_1}(x_1 p) f_{\bar{q}_2}(x_2 p). \tag{6}$$

Focusing on the hadron production in one-dimension p_T space at midrapidity $y = 0$, the momentum distribution function becomes one-dimensional distribution $f(p_T) \equiv dN/dp_T$. The above two formulas therefore reduce to

$$f_{B_j}(p_T) = \kappa_{B_j} f_{q_1}(x_1 p_T) f_{q_2}(x_2 p_T) f_{q_3}(x_3 p_T), \tag{7}$$

$$f_{M_j}(p_T) = \kappa_{M_j} f_{q_1}(x_1 p_T) f_{\bar{q}_2}(x_2 p_T), \tag{8}$$

which are the starting formulas of deriving $\langle p_T \rangle$ of hadrons in this paper. Coefficients κ_{B_j} and κ_{M_j} are independent of p_T and therefore are not involved in derivation of the $\langle p_T \rangle$ of hadrons. Their detailed expressions can be found in Ref. [38]. Equations (7) and (8) lead to some interesting correlations among the production of different hadrons such as QNS mentioned above, which were tested by experimental data [39,41–45]. Our previous works [37,40,41,43,45] have shown that Eqs. (7) and (8) are quite effective in describing the p_T distribution and elliptic flow of light-flavor and single-charm hadrons.

The $\langle p_T \rangle$ value is dominated by the p_T spectrum of particles in the low p_T range. Therefore, we focus on p_T spectra of quarks and antiquarks with low p_T. Unfortunately, quarks of low p_T are governed by nonperturbative QCD dynamics and their distributions are difficult to be calculated from first principles. Considering that the experimental data for the p_T spectra of hadrons at midrapidity in the low p_T range in relativistic heavy-ion collisions are generally well fitted by the exponential function and/or Boltzmann distribution [14,15,17,18,21,22], in this paper we take the following parametrization for quark p_T spectra at midrapidity:

$$f_{q_i}(p_T) = \mathcal{N} p_T^k \exp\left[-\frac{\sqrt{p_T^2 + m_i^2}}{T_i}\right], \tag{9}$$

which is convenient to derive analytic results of hadronic $\langle p_T \rangle$. Here, $\mathcal{N}$ is the coefficient to quantify the number of q_i, which is irrelevant to $\langle p_T \rangle$ calculations. T_i is the slope parameter to quantify the exponential decrease of the spectrum. Exponent k tunes the behavior of the spectrum at small p_T. In the case of two-dimensional Boltzmann distribution, in the stationary system, we have $k = 1$ and in the one-dimensional case we have $k = 0$. If we directly apply Eq. (9) to fit the experimental data of p_T spectra of hadrons by Eq. (7), we should take $k \approx 1/3$ to properly describe baryon and $k \approx 1/2$ to properly describe meson (mainly ϕ). In addition, the effect of strong collective radial flow should be included in the quark spectrum in the laboratory frame, which is dependent on collision energies in relativistic heavy-ion collisions. With these considerations, we take k as a free parameter in the range [0,1] in this study of the hadronic $\langle p_T \rangle$ in relativistic heavy-ion collisions at RHIC and LHC energies.

Substituting Eq. (9) into Eqs. (7) and (8), we obtain

$$\begin{aligned}\langle p_T \rangle_B &= \frac{\int f_B(p_T) p_T dp_T}{\int f_B(p_T) dp_T} \\ &= \frac{\int p_T^{3k+1} \exp\left[-\left(\frac{x_1}{T_1} + \frac{x_2}{T_2} + \frac{x_3}{T_3}\right)\sqrt{p_T^2 + m_B^2}\right] dp_T}{\int p_T^{3k} \exp\left[-\left(\frac{x_1}{T_1} + \frac{x_2}{T_2} + \frac{x_3}{T_3}\right)\sqrt{p_T^2 + m_B^2}\right] dp_T},\end{aligned} \tag{10}$$

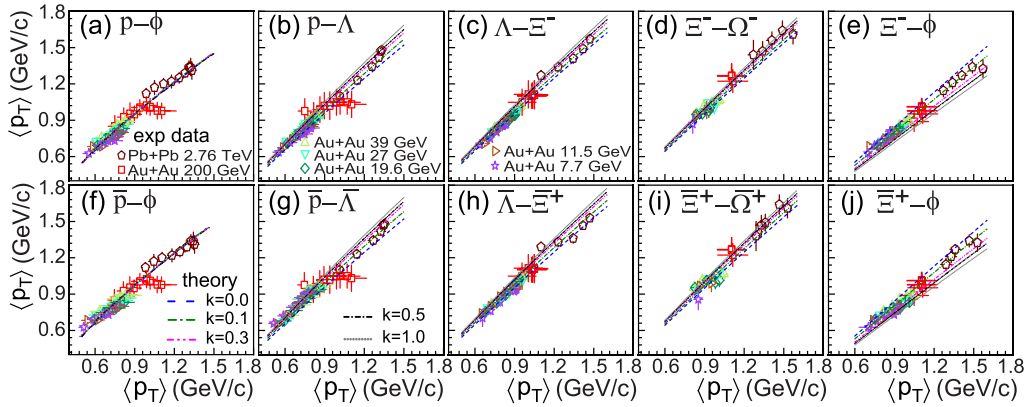

FIG. 1. $\langle p_T\rangle$ correlations of hadrons at midrapidity in relativistic heavy-ion collisions at different collision energies and in different collision centralities. The label h_i–h_j denotes that $\langle p_T\rangle$ of h_i is shown in horizontal axis and that of h_j is shown in vertical axis. Symbols are experimental data [14,15,17–22,46] with quadratic combination of statistical and systematic uncertainties. Lines of different types are theoretical results with parameter values in Table I.

$$\langle p_T\rangle_M = \frac{\int f_M(p_T)p_T dp_T}{\int f_M(p_T)dp_T} = \frac{\int p_T^{2k+1}\exp\left[-\left(\frac{x_1}{T_1}+\frac{x_2}{T_2}\right)\sqrt{p_T^2+m_M^2}\right]dp_T}{\int p_T^{2k}\exp\left[-\left(\frac{x_1}{T_1}+\frac{x_2}{T_2}\right)\sqrt{p_T^2+m_M^2}\right]dp_T}, \quad (11)$$

where $m_B = m_{q_1}+m_{q_2}+m_{q_3}$ and $m_M = m_{q_1}+m_{\bar{q}_2}$. We use the integral formula

$$\int_0^\infty p_T^n \exp\left[-a\sqrt{p_T^2+m^2}\right]dp_T = m^{n+1}\frac{2^{n/2}\Gamma\left(\frac{n+1}{2}\right)}{\sqrt{\pi}}\frac{K_{n/2+1}(\alpha)}{\alpha^{n/2}}, \quad (12)$$

where $\alpha = a\,m$, $\Gamma(z)$ is gamma function and $K_n(z)$ is the modified Bessel function of the second kind. We obtain

$$\langle p_T\rangle_B = \left(m_{q_1}+m_{q_2}+m_{q_3}\right)\sqrt{\frac{2}{\alpha_B}}\frac{\Gamma(3k/2+1)}{\Gamma\left(3k/2+\frac{1}{2}\right)} \times\frac{K_{3k/2+3/2}(\alpha_B)}{K_{3k/2+1}(\alpha_B)}, \quad (13)$$

$$\langle p_T\rangle_M = \left(m_{q_1}+m_{\bar{q}_2}\right)\sqrt{\frac{2}{\alpha_M}}\frac{\Gamma(k+1)}{\Gamma(k+\frac{1}{2})}\frac{K_{k+3/2}(\alpha_M)}{K_{k+1}(\alpha_M)}, \quad (14)$$

with

$$\alpha_B = \frac{m_{q_1}}{T_1}+\frac{m_{q_2}}{T_2}+\frac{m_{q_3}}{T_3} = \alpha_{q_1}+\alpha_{q_2}+\alpha_{q_3} \quad (15)$$

and

$$\alpha_M = \frac{m_{q_1}}{T_1}+\frac{m_{\bar{q}_2}}{T_2} = \alpha_{q_1}+\alpha_{\bar{q}_2}. \quad (16)$$

As shown by these expressions, the $\langle p_T\rangle$ of different hadrons is correlated by the simple combination of the slope parameter α_{q_i} of quarks at hadronization.

Bessel function $K_\nu(\alpha)$ and gamma function $\Gamma(z)$ usually have complex expressions. Here, we present the numerical approximations for $\langle p_T\rangle_B$ and $\langle p_T\rangle_M$,

$$\langle p_T\rangle_B \approx \left(m_{q_1}+m_{q_2}+m_{q_3}\right)\times\left(0.26+0.024k+\frac{0.96+2.99k}{\alpha_B}\right), \quad (17)$$

$$\langle p_T\rangle_M \approx \left(m_{q_1}+m_{\bar{q}_2}\right)\left(0.25+0.03k+\frac{0.97+1.99k}{\alpha_M}\right), \quad (18)$$

to see their dependence on α and k in a numerically intuitive way. The relative errors of these two approximations are less than about 3% for the physical range of $\langle p_T\rangle_B$ and $\langle p_T\rangle_M$ in heavy-ion collisions at RHIC and LHC energies studied in this paper.

III. CORRELATIONS AMONG $\langle p_T\rangle$ OF DIFFERENT HADRONS

In this section, we study the correlation among the $\langle p_T\rangle$ of different hadrons. In Fig. 1(a), we present the $\langle p_T\rangle$ of protons as the horizontal axis and $\langle p_T\rangle$ of ϕ at correspondingly collision energy and centrality as the vertical axis to study the correlation between them. As we know, the mass of the proton is close to that of ϕ but the quark flavor composition of the proton (uud) is completely different from that of ϕ ($s\bar{s}$). Except a few datum points in central Au+Au collisions at $\sqrt{s_{NN}} = 200$ GeV, we see a relatively stable correlation between the $\langle p_T\rangle$ of the proton and that of ϕ. In Figs. 1(b)–1(d), we show correlations among protons, Λ, Ξ^-, and Ω^- in the manner of successive strangeness. In Fig. 1(e), we show the correlation between ϕ and Ξ^-, which both have two strange (anti)quarks. We see the systematic correlations among these hadrons. In Figs. 1(f)–1(j), we show the correlation among $\langle p_T\rangle$ data of ϕ and antibaryons and we also find the systematic correlations among them.

As we know, the hot nuclear matters created in heavy-ion collisions at different collision energies and centralities have different size and geometry, different evolution times in the

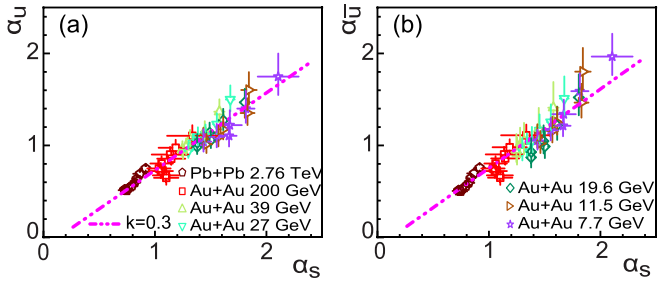

FIG. 2. Correlation between α_u and α_s (a) and that between $\alpha_{\bar{u}}$ and α_s (b), which are extracted from the $\langle p_T \rangle$ data of proton, antiproton, and ϕ [14,15,17,18,21,22], according to Eqs. (19) and (20) at a given $k = 0.3$. The dot-dashed line is the linear fit.

partonic phase, and in the subsequent hadronic rescattering stage, etc. The correlations shown in Fig. 1 seem to assign these differences into a systematic manner and therefore may indicate some underlying physics, which is universal in heavy-ion collision at both RHIC and LHC energies. We think that the universal hadronization mechanism may be a possible physical reason.

Therefore, we apply the EVC model in Sec. II to understand the above correlations in experimental data of hadronic $\langle p_T \rangle$. Hadrons in Fig. 1 are all made up of up, down, strange quarks, and their antiquarks. In our model, the exponent parameter k and slope parameters α_u, α_d, α_s, $\alpha_{\bar{u}}$, $\alpha_{\bar{d}}$, and $\alpha_{\bar{s}}$ need to be fixed to calculate $\langle p_T \rangle$ of hadrons according to Eqs. (13)–(16). Here, we can assume the isospin symmetry between up and down quarks $\alpha_u = \alpha_d$ at midrapidity in relativistic heavy-ion collisions. We also assume the charge conjugation symmetry for strange quarks and antiquarks $\alpha_s = \alpha_{\bar{s}}$, which is found to be a good approximation at midrapidity in relativistic heavy-ion collisions at RHIC and LHC energies [38]. Finally, only three slope parameters α_u, $\alpha_{\bar{u}}$, and α_s are left in addition to the exponent parameter k.

If we know the correlation between α_u and α_s, we can calculate the correlations among the $\langle p_T \rangle$ of baryons and ϕ, and therefore use them to explain experimental data in Figs. 1(a)–1(e). Applying Eqs. (13) and (14) to proton and ϕ, we have

$$\langle p_T \rangle_p = 3m_u \sqrt{\frac{2}{\alpha_p}} \frac{\Gamma(3k/2+1)}{\Gamma(3k/2+\frac{1}{2})} \frac{K_{3k/2+3/2}(\alpha_p)}{K_{3k/2+1}(\alpha_p)}, \quad (19)$$

$$\langle p_T \rangle_\phi = 2m_s \sqrt{\frac{2}{\alpha_\phi}} \frac{\Gamma(k+1)}{\Gamma(k+\frac{1}{2})} \frac{K_{k+3/2}(\alpha_\phi)}{K_{k+1}(\alpha_\phi)}, \quad (20)$$

where

$$\alpha_p = 2\alpha_u + \alpha_d = 3\alpha_u, \quad (21)$$

$$\alpha_\phi = \alpha_s + \alpha_{\bar{s}} = 2\alpha_s, \quad (22)$$

according to Eqs. (15) and (16). By fitting experimental data of $\langle p_T \rangle$ of proton and ϕ shown in Fig. 1(a), we can reversely extract the correlation between α_u and α_s. In Fig. 2(a), we show results of α_u and α_s at a given $k = 0.3$ as an example, which can be parameterized as

$$\alpha_u(\alpha_s) = c_0 + c_1\alpha_s, \quad (23)$$

TABLE I. Coefficients in Eqs. (23) and (24) at different k, which are extracted from experimental data of $\langle p_T \rangle$ of (anti)proton and ϕ at midrapidity in heavy-ion collisions at RHIC and LHC energies [14,15,17,18,18,21,22].

k	c_0	c_1	d_0	d_1
0.0	−0.05	0.69	−0.05	0.71
0.1	−0.07	0.76	−0.07	0.78
0.3	−0.11	0.84	−0.11	0.86
0.5	−0.15	0.89	−0.15	0.91
1.0	−0.23	0.94	−0.25	0.97

where c_0 and c_1 are two coefficients. Because the extraction is dependent on the exponent parameter k, we list the values of c_0 and c_1 at several different k in Table I. The resulting fitted correlations between proton and ϕ with these different extractions are shown as lines with different types in Fig. 1(a). To reduce the bias in choice of k, we let these different extractions to represent the same correlation between $\langle p_T \rangle$ of proton and ϕ, i.e., these lines are coincident with each other. By fitting experimental data of the $\langle p_T \rangle$ of antiproton and ϕ, we also obtain the correlation between $\alpha_{\bar{u}}$ and α_s in Fig. 2(b) with the parameterized form

$$\alpha_{\bar{u}}(\alpha_s) = d_0 + d_1\alpha_s. \quad (24)$$

The values of coefficients d_0 and d_1 at several k are shown in Table I and the corresponding fit is shown in Fig. 1(f). At low RHIC energies where α_s is large, $\alpha_{\bar{u}}$ is different from α_u to a certain extent, which is because the finite baryon density at low collision energies will cause the asymmetry between up/down quarks and their antiquarks.

With these two relationships, we can calculate correlations among $\langle p_T \rangle$ of various hadrons by Eqs. (13) and (14) with Eqs. (21), (22), and

$$\alpha_\Lambda = 2\alpha_u + \alpha_s, \quad (25)$$

$$\alpha_\Xi = 2\alpha_s + \alpha_u, \quad (26)$$

$$\alpha_\Omega = 3\alpha_s, \quad (27)$$

and the corresponding antibaryons according to Eqs. (15) and (16). In Fig. 1, we present theoretical results for the $\langle p_T \rangle$ correlations of $p\Lambda$, $\Lambda\Xi^-$, $\Xi^-\Omega^-$, and $\Xi^-\phi$ pairs, and those of antibaryons. Results at different k with corresponding coefficients in Table I are shown as lines with different types. These lines are different to a certain extent, which shows the theoretical uncertainties due to the selection of the exponent parameter k. Overall, we see that the systematic feature of the correlations exhibited by the $\langle p_T \rangle$ data of these hadrons can be described by our model.

This result is quite interesting. Here we only consider the effect of hadronization by EVC mechanism without any considerations on other dynamical ingredients such as the system size and geometry, evolution time, hadronic rescattering, etc. We run the event generators URQMD 3.4 [8] and AMPT 2.26 (1.26) [10], which practically include those dynamical processes, and we do not find a better description on the systematic correlations in Fig. 1 when we use the default parameter values of event generators. Therefore, our results

in Fig. 1 indicate the important role of hadronization by EVC mechanism in describing the $\langle p_T \rangle$ of those hadrons in relativistic heavy-ion collisions at both RHIC and LHC energies.

IV. $\langle p_T \rangle$ OF HADRONS AS A FUNCTION OF $(dN_{\rm ch}/dy)/(0.5N_{\rm part})$

Experimental data for hadronic $\langle p_T \rangle$ shown in the form of Fig. 1 reveal the correlations among $\langle p_T \rangle$ of different hadrons, which are mainly relevant to the hadronization mechanism according to our studies in the previous section. In this section, we study another aspect of $\langle p_T \rangle$ of hadrons, i.e., their absolute values, and search some regularity underlying these experimental data in heavy-ion collisions at RHIC and LHC energies.

There are many physical ingredients that influence the $\langle p_T \rangle$ of hadrons. Generally speaking, there are two main sources of generating the transverse momentum of hadrons. The first source is the intensive parton interactions at the early collision stage which form the thermal bulk nuclear matter and generate primordial thermal or stochastic momentum of particles. Another source is the expansion of hot nuclear matter in both the partonic phase and hadronic phase, which generates the collective radial flow and therefore strengthens the $\langle p_T \rangle$ of hadrons. The effects of these two sources are both influenced by collision parameters such as collision energy, collision centrality, and collision system. These collision parameters influence the size and geometry of the bulk nuclear matter, the intensity of soft parton/particle interactions, the time of system expansion, and, correspondingly, the magnitude of collective radial flow. In view of these complex ingredients, it seems to be difficult to find a simple and perfect regularity for the $\langle p_T \rangle$ of hadrons by directly analyzing the experimental data of $\langle p_T \rangle$ of hadrons in relativistic heavy-ion collisions.

Here, we try to take $(dN_{\rm ch}/dy)/(0.5N_{\rm part})$ to quantify the excitation of hadronic $\langle p_T \rangle$. $dN_{\rm ch}/dy$ is the rapidity density of charged particles at midrapidity. It can characterize the size of the created hot nuclear matter. In a general case, i.e., as other conditions (such as collision energy and collision system) are not changed, the larger system means more intensive particle excitation (i.e., higher stochastic momentum or higher temperature) and more expansion (i.e., more radial flow). Experimental observations have shown that the $\langle p_T \rangle$ of hadrons generally positively responds to the $dN_{\rm ch}/dy$ at given collision energy and collision system [14,15,17,18,21,22,46–48]. Therefore, we take $dN_{\rm ch}/dy$ as the main relevant ingredient parametrizing $\langle p_T \rangle$ of hadrons. $N_{\rm part}$ is the number of participant nucleons calculated in the Glauber model [49], which depends on the collision energy, collision system, and impact parameter. It can characterize the total amount of energy deposited in the collision region and therefore characterize the initial size and energy density of the created nuclear matter. The ratio $(dN_{\rm ch}/dy)/(0.5N_{\rm part})$ quantifies the average number of charged particles produced by a pair of participant nucleons. It can roughly characterize the average number of charged particles produced by a unit effective energy deposited by the collision of a pair of nucleons. In general, a higher $(dN_{\rm ch}/dy)/(0.5N_{\rm part})$ means more intensive particle excitation which needs more intensive parton interactions and also means more momentum generation. Therefore, we expect that $(dN_{\rm ch}/dy)/(0.5N_{\rm part})$ should positively correlate with the $\langle p_T \rangle$ of hadrons.

The geometry property of hot nuclear matter, mainly controlled by impact parameter, also influences the $\langle p_T \rangle$ of hadrons. In particular, in peripheral collisions where the impact parameter is large, various-order anisotropic flows are generated and will influence the $\langle p_T \rangle$ to a certain extent by, for example, the asymmetric distribution of p_x and p_y. Therefore, to remove the freedom of the impact parameter which is quite complex to parametrize, we only use the experimental data of hadronic $\langle p_T \rangle$ in central collisions to search their possible regularity with respect to $(dN_{\rm ch}/dy)/(0.5N_{\rm part})$.

In Fig. 3, we compile the experimental data for $\langle p_T \rangle$ of ϕ and (anti)baryons at midrapidity in central heavy-ion collisions at different collision energies. We see that these data of hadronic $\langle p_T \rangle$ exhibit a clear regularity when we plot them as a function of $(dN_{\rm ch}/dy)/(0.5N_{\rm part})$. Here data of $dN_{\rm ch}/dy$ at midrapidity and $N_{\rm part}$ are taken from Refs. [15–17,22]. In the calculation of $(dN_{\rm ch}/dy)/(0.5N_{\rm part})$, only experimental uncertainties of $dN_{\rm ch}/dy$ are included.

According to the behavior of experimental data in Fig. 3 and the approximated formula of hadronic $\langle p_T \rangle$ in Eqs. (17) and (18), we parametrize the $(dN_{\rm ch}/dy)/(0.5N_{\rm part})$ dependence of slope parameter α_q of quarks as the following form:

$$\alpha_q = \left[g_q + h_q \left(\frac{dN_{\rm ch}/dy}{N_{\rm part}/2} \right)^{2/3} \right]^{-1}. \tag{28}$$

Coefficients g and h of u, $\bar{u}$, and s quarks can be fixed by using Eqs. (13) and (14) to fit the experimental data of proton, antiproton, and $\Omega^- + \bar{\Omega}^+$. Values of g and h at different k are shown in Table II. These fittings to experimental data of proton, antiproton, and $\Omega^- + \bar{\Omega}^+$ are shown in Figs. 3(a), 3(e) and 3(h) as lines of different types. To avoid the bias in selection of the exponent parameter k, we let these different fitting groups generate the same $(dN_{\rm ch}/dy)/(0.5N_{\rm part})$ dependence for $\langle p_T \rangle$ of proton, antiproton, and $\Omega^- + \bar{\Omega}^+$, that is, lines of different types are coincident with each other in Figs. 3(a), 3(e) and 3(h). This treatment can enable us to study theoretical uncertainty in prediction of other hadrons. Results for $\langle p_T \rangle$ of other hadrons as the function of $(dN_{\rm ch}/dy)/(0.5N_{\rm part})$ are shown in Figs. 3(b)–3(d) and 3(f) and 3(g).

We see that theoretical results of hyperons at different k in Figs. 3(b) and 3(c) and 3(f) and 3(g) are coincident with each other and they are in good agreement with experimental data. Results of ϕ in Fig. 3(d) are dependent on k to a certain extent. In these results at different k, we see that the results of ϕ at $k = 0.1, 0.3$ are globally better than others. This feature is similar with that in correlations of hadronic $\langle p_T \rangle$ in Fig. 1.

V. INFLUENCE OF RESONANCE DECAY

In previous calculations, results of hadronic $\langle p_T \rangle$ are those for initially produced hadrons by hadronization and effects of resonance decay are not yet included. For protons, Λ, and Ξ^-, a certain fraction of these hadrons observed in experiments comes from decay of higher-mass resonances such as those from decuplet baryons Δ, Σ^* and Ξ^*, respectively. Ω^- and ϕ

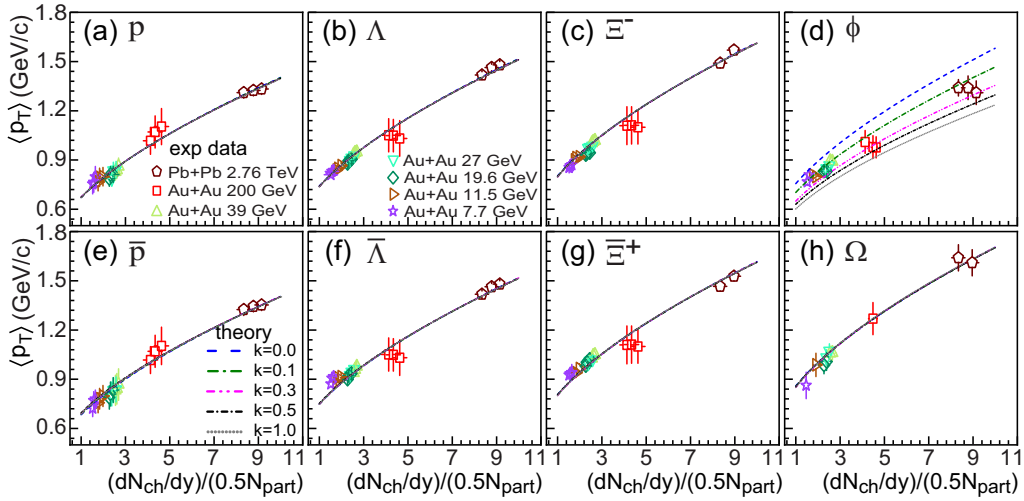

FIG. 3. $\langle p_T \rangle$ of hadrons the function of $(dN_{\rm ch}/dy)/(0.5N_{\rm part})$ at midrapidity in central heavy-ion collisions at different collision energies. Symbols are experimental data [14–22,46] and lines with different types are theoretical results with parameter values in Table II.

are generally expected to be less influenced. In this section, we study the influence of the resonance decay on the correlations among $\langle p_T \rangle$ of different hadrons.

We apply the quark combination model developed in previous works [37,39] to calculate the influence of resonance decay on $\langle p_T \rangle$ of hadrons. The production weight of baryon resonances Δ, Σ^*, and Ξ^* is specifically tuned in the model according to their experimental data in high energy pp and pPb collisions [50,51]. Following experimental corrections, results of Λ and Ξ^- do not include weak decay contributions but results of proton and antiproton include them. We adopt the following strategy to quantify the effect of resonance decays. First, we use the model to calculate the $\langle p_T \rangle$ of the final-state (anti)proton and that of ϕ with the parameterized quark p_T spectra in Eq. (9). We apply the model to fit the $\langle p_T \rangle$ correlation between experimental data of (anti)protons and those of ϕ to obtain the correlation between α_u and α_s with the parametrization form Eq. (23) and that between $\alpha_{\bar{u}}$ and α_s with Eq. (24). The newly obtained coefficients c_0, c_1, d_0, d_1 are slightly different from those in Table I due to the effect of resonance decays. In the fitting process, we keep the same $p\phi$ and $\bar{p}\phi$ correlations shown as lines in Fig 1. Second, we calculate $\langle p_T \rangle$ correlations among other hadron pairs and compare them with the results in Fig. 1 to study the effect of resonance decays. In a similar way, we can also study the effect of resonance decays on the hadronic $\langle p_T \rangle$ as the function of $(dN_{\rm ch}/dy)/(0.5N_{\rm part})$ in central heavy-ion collisions. Here, experimental data of protons, antiprotons, and Ω^- are used to determine the parameters of (anti)quarks and then the results for Λ, $\bar{\Lambda}$, Ξ^-, $\bar{\Xi}^+$, and ϕ are model predictions.

In comparison with the correlation results of directly produced hadrons shown in Fig. 1, the line for $p\Lambda$ correlation with resonance decays rises about 1%, $\Lambda\Xi^-$ correlation has almost no change, $\Xi^-\Omega^-$ correlation falls about 1%, and $\Xi^-\phi$ correlation also falls about 1%. The same change is observed for correlations among antibaryons and ϕ. In comparison with the $(dN_{\rm ch}/dy)/(0.5N_{\rm part})$ dependence of directly produced hadrons shown in Fig. 3, the dependence lines for Λ and $\bar{\Lambda}$ with resonance decays fall about 1% and those for Ξ^- and $\bar{\Xi}^+$ also fall about 1%. These results therefore indicate a weak influence of resonance decays on the $\langle p_T \rangle$ correlation of (anti)baryons and ϕ.

TABLE II. Coefficients in Eq. (28) at different k, which are extracted from experimental data of $\langle p_T \rangle$ of (anti)proton and Ω at midrapidity in heavy-ion collisions at RHIC and LHC energies [14,15,17,18,18,21,22].

	u		$\bar{u}$		s	
k	g	h	g	h	g	h
0.0	0.88	0.68	0.93	0.67	0.60	0.46
0.1	0.64	0.52	0.69	0.52	0.42	0.36
0.3	0.42	0.36	0.45	0.35	0.26	0.25
0.5	0.30	0.27	0.34	0.27	0.19	0.19
1.0	0.18	0.17	0.20	0.17	0.11	0.12

VI. SUMMARY AND DISCUSSION

In this paper, we have applied the quark combination model with EVC approximation to study the averaged transverse momentum ($\langle p_T \rangle$) correlations of proton, Λ, Ξ^-, Ω^-, and ϕ in relativistic heavy-ion collisions. We derived analytic formulas of hadronic $\langle p_T \rangle$ in the case of exponential form of quark p_T spectra at hadronization, which can clarify the correlations among $\langle p_T \rangle$ of identified hadrons based on the constituent quark structure of hadrons. We used these analytic formulas to explain the systematic correlations exhibited in $\langle p_T \rangle$ data of $p\Lambda$, $\Lambda\Xi^-$, $\Xi^-\Omega^-$, and $\Xi^-\phi$ pairs and those of antibaryons. We discussed the regularity for $\langle p_T \rangle$ of these hadrons as the function of $(dN_{\rm ch}/dy)/(N_{\rm part}/2)$ at midrapidity in central heavy-ion collisions at both RHIC and LHC energies, and used our model to self-consistently explain $\langle p_T \rangle$ of these hadrons as the function of $(dN_{\rm ch}/dy)/(N_{\rm part}/2)$. In these studies, we use the experimental data of (anti)protons

to fix the property of up/down (anti)quarks and those of Ω or ϕ to fix that of strange quarks at hadronization. Then we predict the correlations among $\langle p_T \rangle$ of other hadron pairs and compare with experimental data to test the theoretical consistency. Moreover, we studied the effects of resonance decays on $\langle p_T \rangle$ correlations of hadrons and find they are weak in comparison with hadronization.

Our studies have shown that the $\langle p_T \rangle$ correlations among experimental data of proton, Λ, Ξ^-, Ω^-, and ϕ in Au+Au collisions at RHIC energies and Pb+Pb collisions at $\sqrt{s_{NN}} =$ 2.76 TeV can be self-consistently described by the EVC mechanism of constituent quarks and antiquarks at hadronization. This indicates the important role of constituent quarks and antiquarks as the effective degrees of freedom of the hot nuclear matter at the hadronization stage and their EVC as the main feature of hadron formation in relativistic heavy-ion collisions. The current paper is consistent with our previous works in studying the elliptic flow of these hadrons and the QNS property of p_T spectra of Ω^- and ϕ in relativistic heavy-ion collisions at RHIC and LHC energies using the same quark combination mechanism [42,43].

In relativistic heavy-ion collisions, rescatterings of hadrons after hadronization will influence momentum of hadrons to a certain extent. For example, the signal of ϕ may be lost by the scattering of their decay daughters with the surrounding hadrons and ϕ may also be generated by the coalescence of two kaon. We will study this hadronic rescattering effect in future work. In addition, we will also carry out a systematic study on p_T spectra of identified hadrons at midrapidity in different centralities in Au+Au collisions at STAR BES energies. p_T spectra of identified hadrons contain more dynamical information than their $\langle p_T \rangle$, which can be used to further test our quark combination model at low RHIC energies.

ACKNOWLEDGMENTS

We thank Prof. X. L. Zhu for providing us the experimental data of hadronic $\langle p_T \rangle$ in Au+Au collisions at RHIC energies. This work is supported in part by Shandong Provincial Natural Science Foundation (Grants No. ZR2019YQ06 and No. ZR2019MA053), the National Natural Science Foundation of China under Grants No. 11975011 and No. 12175115, and Higher Educational Youth Innovation Science and Technology Program of Shandong Province (Grant No. 2019KJJ010).

[1] U. W. Heinz and M. Jacob, arXiv:nucl-th/0002042.
[2] I. Arsene *et al.* (BRAHMS Collaboration), Nucl. Phys. A **757**, 1 (2005).
[3] K. Adcox *et al.* (PHENIX Collaboration), Nucl. Phys. A **757**, 184 (2005).
[4] B. B. Back *et al.* (PHOBOS Collaboration), Nucl. Phys. A **757**, 28 (2005).
[5] J. Adams *et al.* (STAR Collaboration), Nucl. Phys. A **757**, 102 (2005).
[6] M. Gyulassy and L. McLerran, Nucl. Phys. A **750**, 30 (2005).
[7] P. F. Kolb and U. Heinz, *Quark–Gluon Plasma 3* (World Scientific, Singapore, 2004), pp. 634–714.
[8] S. A. Bass *et al.*, Prog. Part. Nucl. Phys. **41**, 255 (1998).
[9] S. A. Bass and A. Dumitru, Phys. Rev. C **61**, 064909 (2000).
[10] Z.-W. Lin, C. M. Ko, B.-A. Li, B. Zhang, and S. Pal, Phys. Rev. C **72**, 064901 (2005).
[11] K. Adcox *et al.*(PHENIX Collaboration), Phys. Rev. Lett. **88**, 242301 (2002).
[12] K. Adcox *et al.* (PHENIX Collaboration), Phys. Rev. Lett. **88**, 022301 (2001).
[13] B. I. Abelev *et al.* (STAR Collaboration), Phys. Rev. Lett. **97**, 152301 (2006).
[14] B. I. Abelev *et al.* (STAR Collaboration), Phys. Rev. C **79**, 064903 (2009).
[15] B. I. Abelev *et al.* (STAR Collaboration), Phys. Rev. C **79**, 034909 (2009).
[16] K. Aamodt *et al.* (ALICE Collaboration), Phys. Rev. Lett. **106**, 032301 (2011).
[17] B. Abelev *et al.* (ALICE Collaboration), Phys. Rev. C **88**, 044910 (2013).
[18] B. B. Abelev *et al.* (ALICE Collaboration), Phys. Rev. C **91**, 024609 (2015).
[19] B. B. Abelev *et al.* (ALICE Collaboration), Phys. Rev. Lett. **111**, 222301 (2013).
[20] B. B. Abelev *et al.* (ALICE Collaboration), Phys. Lett. B **728**, 216 (2014); Erratum: **734**, 409 (2014).
[21] J. Adam *et al.* (STAR Collaboration), Phys. Rev. C **102**, 034909 (2020).
[22] L. Adamczyk *et al.* (STAR Collaboration), Phys. Rev. C **96**, 044904 (2017).
[23] R. J. Fries, B. Müller, C. Nonaka, and S. A. Bass, Phys. Rev. Lett. **90**, 202303 (2003).
[24] V. Greco, C. M. Ko, and P. Lévai, Phys. Rev. Lett. **90**, 202302 (2003).
[25] R. C. Hwa and C. B. Yang, Phys. Rev. C **67**, 034902 (2003).
[26] P. Huovinen and P. V. Ruuskanen, Annu. Rev. Nucl. Part. Sci. **56**, 163 (2006).
[27] L.-W. Chen and C. M. Ko, Phys. Rev. C **73**, 044903 (2006).
[28] M. Gyulassy, I. Vitev, X.-N. Wang, and B.-W. Zhang, Quark-Gluon Plasma **3**, 123 (2004).
[29] I. P. Lokhtin and A. M. Snigirev, Eur. Phys. J. C **45**, 211 (2006).
[30] B.-W. Zhang, E. Wang, and X.-N. Wang, Phys. Rev. Lett. **93**, 072301 (2004).
[31] Z. Tang, Y. Xu, L. Ruan, G. van Buren, F. Wang, and Z. Xu, Phys. Rev. C **79**, 051901(R) (2009).
[32] L. Ravagli, H. van Hees, and R. Rapp, Phys. Rev. C **79**, 064902(R) (2009).
[33] H. Song, S. A. Bass, U. Heinz, T. Hirano, and C. Shen, Phys. Rev. C **83**, 054910 (2011); **86**, 059903(E) (2012).
[34] W. Cassing and E. L. Bratkovskaya, Phys. Rev. C **78**, 034919 (2008).
[35] I. A. Karpenko, Y. M. Sinyukov, and K. Werner, Phys. Rev. C **87**, 024914 (2013).
[36] Z.-w. Lin and D. Molnar, Phys. Rev. C **68**, 044901 (2003).

[37] J. Song, X.-r. Gou, F.-l. Shao, and Z.-T. Liang, Phys. Lett. B **774**, 516 (2017).
[38] J. Song, X.-F. Wang, H.-H. Li, R.-Q. Wang, and F.-L. Shao, Phys. Rev. C **103**, 034907 (2021).
[39] X.-r. Gou, F.-l. Shao, R.-q. Wang, H.-h. Li, and J. Song, Phys. Rev. D **96**, 094010 (2017).
[40] H.-H. Li, F.-L. Shao, J. Song, and R.-Q. Wang, Phys. Rev. C **97**, 064915 (2018).
[41] J.-w. Zhang, H.-h. Li, F.-l. Shao, and J. Song, Chin. Phys. C **44**, 014101 (2020).
[42] J. Song, F.-l. Shao, and Z.-t. Liang, Phys. Rev. C **102**, 014911 (2020).
[43] J. Song, H.-h. Li, and F.-l. Shao, Eur. Phys. J. C **81**, 1 (2021).
[44] H.-h. Li, F.-l. Shao, and J. Song, Chin. Phys. C **45**, 113105 (2021).
[45] J. Song, H.-h. Li, and F.-l. Shao, Phys. Rev. D **105**, 074027 (2022).
[46] M. Estienne (STAR Collaboration), J. Phys. G: Nucl. Part. Phys. **31**, S873 (2005).
[47] K. K. Olimov, F.-H. Liu, K. A. Musaev, A. K. Olimov, B. J. Tukhtaev, N. S. Saidkhanov, B. S. Yuldashev, K. Olimov, and K. G. Gulamov, Int. J. Mod. Phys. E **30**, 2150029 (2021).
[48] M. Petrovici, I. Berceanu, A. Pop, M. Târzilă, and C. Andrei, Phys. Rev. C **96**, 014908 (2017).
[49] M. L. Miller, K. Reygers, S. J. Sanders, and P. Steinberg, Annu. Rev. Nucl. Part. Sci. **57**, 205 (2007).
[50] B. I. Abelev *et al.* (STAR Collaboration), Phys. Rev. Lett. **97**, 132301 (2006).
[51] D. Adamová *et al.* (ALICE Collaboration), Eur. Phys. J. C **77**, 389 (2017).